Optics & Laser Technology 70 (2015) 71–75

Contents lists available at ScienceDirect

Optics & Laser Technology

journal homepage: www.elsevier.com/locate/optlastec

Ultrafast thermalisation dynamics in an Au film excited by a polarization-shaped femtosecond laser double-pulse

Yan Ou, Qing Yang, Guangqing Du*, Feng Chen*, Yanmin Wu, Yu Lu, Xun Hou

State Key Laboratory for Manufacturing Systems Engineering & Key Laboratory of Photonics Technology for Information, Xi'an Jiaotong University, 710049, China

ARTICLE INFO

Article history:
Received 20 October 2014
Received in revised form
5 January 2015
Accepted 26 January 2015
Available online 14 February 2015

Keywords:
Ultrafast thermalisation dynamics
Double-pulse
Polarization combinations

ABSTRACT

We theoretically investigated the ultrafast non-equilibrium thermalisation dynamics in an Au film irradiated by a polarization-shaped femtosecond laser double-pulse. A non-equilibrium thermal relaxation model is proposed to study the relevance of the polarization of the double-pulse energy that couples to the Au film target. The phonon temperature can be greatly increased by optimizing double-pulse polarization combinations. The results are explained by an enhanced laser energy coupling with the Au film due to a synergetic effect arising from pulse-to-pulse polarization relevance. The study provides a basis for understanding ultrafast thermalisation dynamics for optimizing laser micro- and nano-fabrications by tailoring the polarization state of temporally shaped femtosecond lasers.

1. Introduction

Femtosecond laser processing of materials has been demonstrated to be a powerful tool in micro-patterning for the fabrication of micro- and nano-functional devices, such as micro-optical elements [1,2], microfluidic devices [3,4], and microsensors [5]. Femtosecond laser ablation of materials has significant advantages over long pulse laser ablation such as high precision, high resolution due to minimal heating, and little collateral damage produced during processing [6–8]. In recent years, it has been observed that ablation accuracy can be deteriorated from the thermal effects that originate from multi-pulsed ablation using conventional femtosecond lasers such as a femtosecond laser amplifier [9–11]. It has been explained through the difference in time scales between the pulse separation (~ms) for a femtosecond laser amplifier and the characteristic thermal diffusion cycle (ps–ns). As a result, several methods have been developed to improve processing quality. For example, liquid-assisted femtosecond laser processing can improve the processing quality because liquid can effectively reduce the debris generated during machining processing. However, there are still some inherent problems that exist in these methods such as the energy loss due to laser energy-absorption by water, laser light scattering by gas bubbles in a liquid, and so on [12].

Recently, it was demonstrated that temporally shaped femtosecond laser pulses have a large advantage in improving the manufacturing quality [13–19]. It is experimentally observed that the ablation process can be precisely controlled by optimizing the parameters of pulse train, such as the number of pulses [13,14], the pulse separation [15], and pulse energy ratio [16]. Jiang et al. reported that the maximum electron temperature for femtosecond laser ablation of a metal is decreased and the electron–phonon relaxation period is prolonged by using temporally shaped femtosecond laser pulses [17]. Sim et al. investigated the influence of temporally shaped femtosecond laser pulses on the optical and thermal properties during material ablation [18]. Du et al. revealed that femtosecond laser pulses with the optimal separation are largely advantageous for improving ablation efficiency in laser machining [19]. In fact, the transient electron excitation processes can be relevant to the laser polarization states. As a result, it becomes urgent to clarify the basic dynamics during polarization-shaped femtosecond laser processing of materials. However, it is currently challenging to understand the characteristics of polarization-shaped laser interactions due to the complex dynamics with respect to pulse-to-pulse polarization state combinations.

In this paper, ultrafast thermalisation dynamics of an Au film excited by a polarization-shaped double-pulse is numerically investigated using the finite element method (FEM). With the temperature dependent thermal properties of the Au film, the 2D temperature field evolution in the picosecond time domain was obtained. The results illustrate the dynamics of the energy transfer between the electrons and phonons for different polarization combinations. This is because the polarization-dependent reflectivity on the Au film surface, which can affect the electron–phonon interaction, changes with time. Moreover, the maximum electron temperature, the maximum phonon temperature, and the two temperature relaxation times can be tuned by changing the polarization combinations of the double-pulse and

* Corresponding authors.
E-mail addresses: guangqingdu@mail.xjtu.edu.cn (G. Du), chenfeng@mail.xjtu.edu.cn (F. Chen).

http://dx.doi.org/10.1016/j.optlastec.2015.01.014
0030-3992/

the incident angle. The results provide a theoretical guideline for optimizing the deposition of laser energy into the Au target for micro- and nano-fabrication.

2. Modeling and method

2.1. Two thermal relaxation model

The ultrashort laser-metal interaction can be described by the well-known two temperature model as follows [20]:

$$C_e\frac{\partial T_e}{\partial t}=\nabla(K_e\nabla T_e)-G(T_e-T_p)+Q \tag{1}$$

$$C_p\frac{\partial T_p}{\partial t}=G(T_e-T_p) \tag{2}$$

In the above, T_e is the electron temperature, T_p is the normalized phonon temperature, $K_e=K_0T_e/T_p$ is the temperature-dependent electron heat capacity, $C_e=A_eT_e$ is the electronic heat capacity, C_p is the phonon heat capacity, and G is the electron–phonon coupling strength.

The laser energy absorption rate is written as:

$$Q=S(x,y)\cdot T(t) \tag{3}$$

For a Gaussian spatial distribution of the laser heat source, S is the spatial energy absorption rate, given as:

$$S(x,y)=\sqrt{\frac{4\ln 2}{\pi}}\frac{1-R}{t_p(\delta+\delta_b)}\frac{F}{N}\times\exp\left(-\frac{x}{\delta+\delta_b}-(\frac{y-y_0}{y_s})^2\right) \tag{4}$$

For a multi-pulse sequence, T is the temporal energy absorption rate, which can be described as:

$$T(t)=\sum_{i=1}^{N}\exp\left(-4\ln 2\left(\frac{t-2t_p-(i-1)\Delta}{t_p}\right)^2\right) \tag{5}$$

Where δ is the optical penetration depth, $\delta_b=100$ nm is the electron ballistic transport length for an Au film, t_p is the full width at half maximum (FWHM) pulse duration, F is incident fluence of the pulse train, y_0 is the coordinate of the light front center at the Au film surface, y_s is the profile parameter, N is the pulse number in a train, and Δ is the separation between pulses. The well-known Fresnel formulas give the reflectivity, R, of p and s polarized light as follow [21]:

$$R_S=\left|\frac{\left(\sqrt{(n-ik)^2-\sin^2\theta}-\cos\theta\right)^2}{1-(n-ik)^2}\right|^2 \tag{6}$$

$$R_p=\left|\frac{(n-ik)^2\cos\theta-\sqrt{(n-ik)^2-\sin^2\theta}}{(n-ik)^2\cos\theta-\sqrt{(n-ik)^2-\sin^2\theta}}\right|^2 \tag{7}$$

Here, θ is the incident angle, n is the index of refraction, and k is the extinction coefficient.

2.2. Initial and boundary conditions

The initial temperatures of electrons and phonons are set to room temperature:

$$T_e(x,y,0)=T_p(x,y,0)=300\ K \tag{8}$$

It is reasonable to neglect heat losses from the surface of the metal film. Therefore, the boundary conditions can be expressed as:

$$\left.\frac{\partial T_e}{\partial n}\right|_{\Omega}=\left.\frac{\partial T_p}{\partial n}\right|_{\Omega}=0 \tag{9}$$

Here, Ω represents the four boundary lines of the Au film.

3. Results and discussion

The material parameters for the Au film are as follows [22]: $G=2.6\times10^6$ W/(m^3 K), $A_e=70$ J/m^3 K, $K_0=315$ W/m K, and $C_p=2.5\times10^6$ J/m^3 K. The laser parameters we use are $\lambda=800$ nm and $t_p=100$ fs. The thickness and width of Au film are fixed at 3 μm and 8 μm.

The 2D non-equilibrium temperature field on an Au film surface irradiated by a polarization-shaped double-pulse with the p–p polarization combination (the first pulse and second pulse with the same or different polarization state) is shown in Fig. 1. The electron and phonon are dramatically out of equilibrium at 300 fs. The maximum electron temperature on the Au film surface increases to 6812 K. However, the phonon temperature is undisturbed at this time. At 2 ps, the electron temperature drops sharply and the phonon temperature field distribution becomes visible because of the persistent electron–phonon coupling process. At 3.1 ps, the electron subsystem of the Au film is overheated and the maximum electron temperature on the Au film surface climbs sharply to 8965 K. However, the phonon temperature on the Au film surface goes up to 430 K. The electron temperature field distribution becomes blurred at 10 ps and the phonon temperature field distribution at this time is more distinct. It takes approximately 20 ps to reach thermal equilibrium between the electron and phonon subsystems, and the maximum equilibrium temperature on the Au film surface is close to 820 K. When the laser fluence exceeds the damage threshold, the phase transformations of the heat-affected zone can cause phase explosions leading to material removal.

Fig. 2 shows the transient responses of the reflectivity irradiated by polarization-shaped double-pulses with p–p, s–s, s–p, and p–s polarization combinations. The reflectivity curves exhibit two-valley profiles for the different polarization combinations. The second reflectivity valley is lower than the first one. This originates from the high-temperature electrons excited on the Au film surface after the first pulse, which help lower the surface reflectivity for the second pulse [18]. It can be seen in Fig. 2 that the minimum value of the reflectivity for the p–p polarization combination is lower than that for the s–s polarization combination. In addition, the minimum

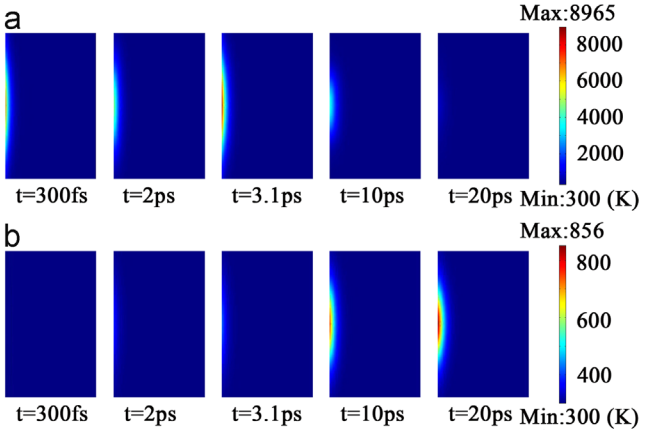

Fig. 1. The 2D non-equilibrium temperature field on an Au film surface irradiated by a polarization-shaped double-pulse with the p–p polarization combination. The incident angle $\theta=30^\circ$, laser fluence $F=0.2$ J/cm^2, pulse duration $t_p=100$ fs, laser wavelength $\lambda=800$ nm, pulse separation $\Delta=3$ ps. (a) The electron temperature field. (b) The phonon temperature field.

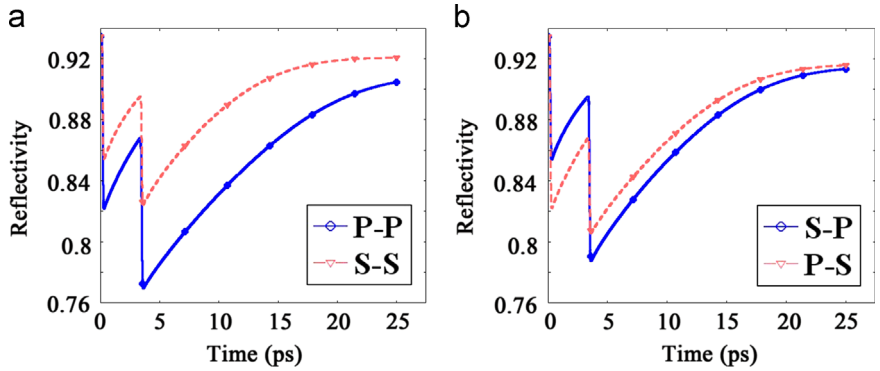

Fig. 2. The transient responses of the reflectivity on the Au film surface irradiated by polarization-shaped double-pulses with p–p, s–s, s–p, and p–s polarization combinations. The incident angle $\theta=50^{\circ}$, laser fluence $F=0.3$ J/cm^2, pulse duration $t_p=100$ fs, laser wavelength $\lambda=800$ nm, pulse separation $\Delta=3.5$ ps. (a) The reflectivity for p–p and s–s polarization combinations. (b) The reflectivity for s–p and p–s polarization combinations.

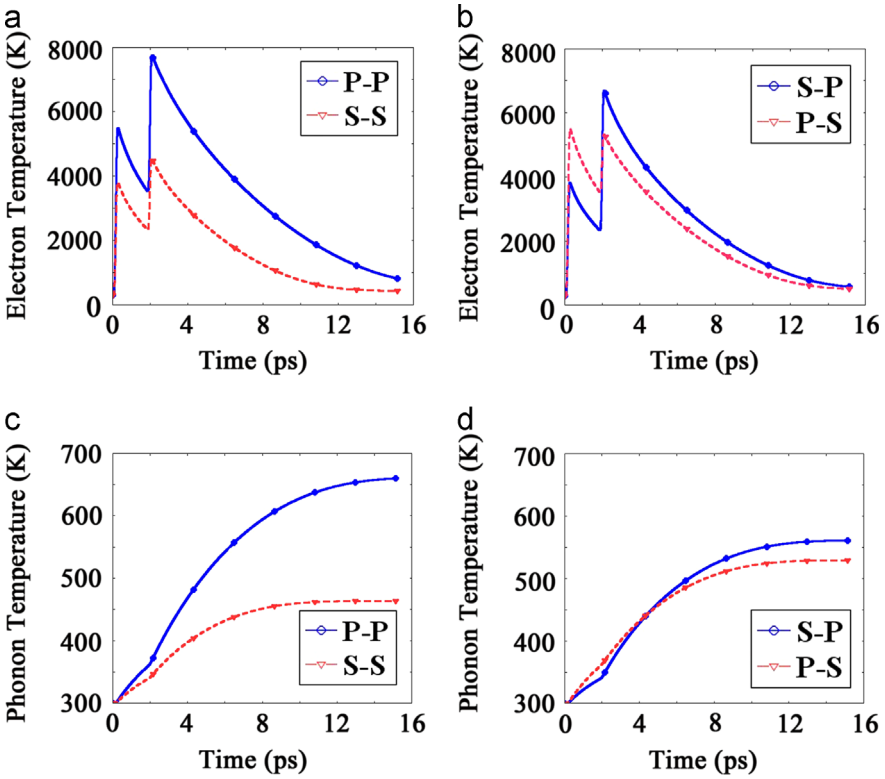

Fig. 3. The maximum electron temperature and phonon temperature on the Au film surface irradiated by polarization-shaped double-pulse with p–p, s–s, s–p, and p–s polarization combinations. The incident angle $\theta=70^{\circ}$, laser fluence $F=0.1$ J/cm^2, pulse duration $t_p=100$ fs, laser wavelength $\lambda=800$ nm, pulse separation $\Delta=2$ ps. (a) and (b) The maximum electron temperature. (c) and (d) The maximum phonon temperature.

value of the reflectivity for the s–p polarization combination is lower than that for the p–s polarization combination. When the incident angle is 50°, laser energy can be more easily coupled into the Au film with a p-polarized laser because the reflectivity irritated by the p-polarized laser is lower than that irritated by an s-polarized laser. As a result, the electron temperature for the p–p polarization combination is higher than that for the s–s polarization combination when the incident angle is 50°. For the s–p polarization combination, the electron state irradiated by the s pulse is too low to absorb the second p pulse energy efficiently resulting in a reduced energy coupling efficiency. In contrast, for the p–s polarization combination, the excited electrons by the first p pulse may be too high to reflect the second s pulse energy. However, the energy coupling efficiency of the s–p polarization is higher than that of the p–s polarization. Therefore, more p pulse energy couples to the electron subsystem due to the increase of the absorption coefficient produced by s polarization. In short, we can control the reflectivity on the Au film surface by changing the polarization combination.

The maximum electron and phonon temperature on the Au film surface irradiated by polarization-shaped double-pulse with p–p, s–s, s–p, and p–s polarization combinations are shown in Fig. 3. The maximum electron temperature reaches a peak of 7748 K, 4551 K, 6685 K and 5318 K for p–p, s–s, s–p, and p–s polarization combinations, respectively. The electron temperature is determined by the absorptive pulse energy. Higher absorptive pulse energy can lead to a higher electron temperature. The absorbed pulse energy from a single p pulse is more than from a single s pulse when the incident angle is 70° [21]. For a double-pulse with p–p polarization, the electron temperature is excited to a higher state because of the higher energy coupling efficiency. More laser energy couples with the electron subsystem for the p–p polarization combination, leading to a higher electron

temperature than that of other double-pulse polarization combinations. The absorbed energy of the Au film from a double-pulse with the s–s polarization combination is less than that from double-pulses with other polarization combinations. As with the s–p polarization combination, the electron state excited by the first s pulse is too low to absorb the second p pulse energy. In addition, the electrons excited by the first p pulse may be too high to reflect the second s pulse for the p–s polarization combination. However, the maximum electron temperature for the s–p polarization combination is higher than that excited by the p–s polarization combination when the incident angle is 70° due to higher energy coupling efficiency. Fig. 3(c) and (d) show that the maximum phonon temperature increases dramatically with time when it is less than 12 ps. After 12 ps, the maximum phonon temperature of Au film surface is almost constant with values of 659 K, 463 K, 560 K and 528 K for p–p, s–s, s–p and p–s polarization combinations, respectively. The phonon temperature for the p–p polarization combination is higher than the other polarization state combinations. This is because the electron temperature for the p–p polarization combination is much higher than that for other polarization state combinations. Thus, more energy can be transferred from the electron subsystem to the phonon subsystem for the p–p polarization combination by the electron–phonon coupling mechanism. Optimizing the polarization combinations of polarization-shaped femtosecond laser pulses will be helpful for improving the efficiency of micromachining.

Fig. 4 shows the maximum electron and phonon temperatures on the Au film surface as a function of the incident angle for polarization-shaped double-pulses for s–p, p–s, p–p, and s–s polarization combinations. The maximum electron and phonon temperature is independent of the polarization combination for incident angles less than 10°. When the incident angle is 70°, the maximum electron temperature on the Au film surface is 9279 K, 7698 K, 11183 K, and 5668 K for s–p, p–s, p–p, and s–s polarization combinations, respectively. The corresponding maximum phonon temperature is 779 K, 711 K, 1035 K, and 552 K, respectively. This is because the electron temperature is determined by the absorbed energy from the laser that is affected by the polarization-dependent reflectivity of the Au film surface. The energy absorptivity for different polarization combinations has the same value at the incident angel of 0°. By changing the incident angle from 0° to 70°, the energy absorptivity for a single p pulse is increased from 30% to 55% while the energy absorptivity for a single s pulse decreases from 30% to 10% [21]. The rate of change of the energy absorptivity for a single p pulse is higher than that for a single s pulse. Therefore, total absorptive energy for s–p, p–s, and p–p polarization combinations increases as the incident angle changes from 0° to 70°. The absorptive energy for the s–s polarization combination decreases gradually as the incident angle goes from 0° to 70°. As a result, the maximum electron temperature gradually decreases with incident angle changing from 0° to 70° for the s–s polarization combination. The maximum electron temperature increases with the incident angle as it changes from 0° to 70° for other polarization combinations. In addition, the maximum electron temperature and phonon temperature change similarly with the incident angle as it goes from 0° to 70°. This is because the higher electron temperature can make more heat transfer from the electron subsystem to the phonon subsystem, leading to a higher phonon temperature. These results will be helpful for determining the optimal conditions for micromachining by controlling the polarization states of double-pulse and incident angle.

Fig. 5 shows the two temperature relaxation time on the Au film surface as a function of the incident angle for polarization-shaped double-pulses with s–p, p–s, p–p, and s–s polarization combinations. The two temperature relaxation time is defined as the period of time that energy transfers from the electron subsystem to the phonon subsystem after femtosecond laser excitations. It is interesting that the different polarization combinations lead to distinct modifications of the two-temperature relaxation time. For the s–s polarization combination, the two-temperature relaxation time decreases with the incident angle as it goes from 0° to 70°. However, the two-temperature relaxation time increases with the incident angle as it changes from 0° to 70° for all other polarization combinations. This is because the energy absorption is determined by the excited electron state. The total absorbed energy affects the electron–phonon relaxation period according to the two-temperature model prediction in our previous investigations [19]. It is generally accepted that a shortened electron–phonon relaxation period leads to a localization of the phonon energy, which causes a high material removal ratio on the Au film surface. Therefore, the localization of energy deposition can be

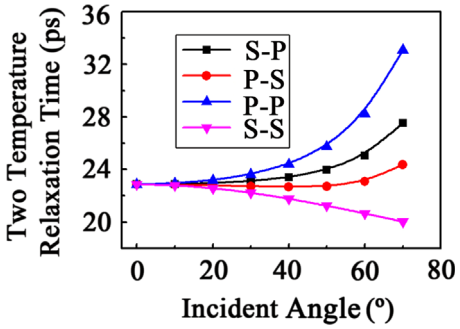

Fig. 5. The two temperature relaxation time on the Au film surface as a function of the incident angle for polarization-shaped double-pulses with s–p, p–s, p–p, and s–s polarization combinations. The laser fluence F=0. 25 J/cm^2, pulse duration t_p=100 fs, laser wavelength λ=800 nm, pulse separation Δ=2.5 ps.

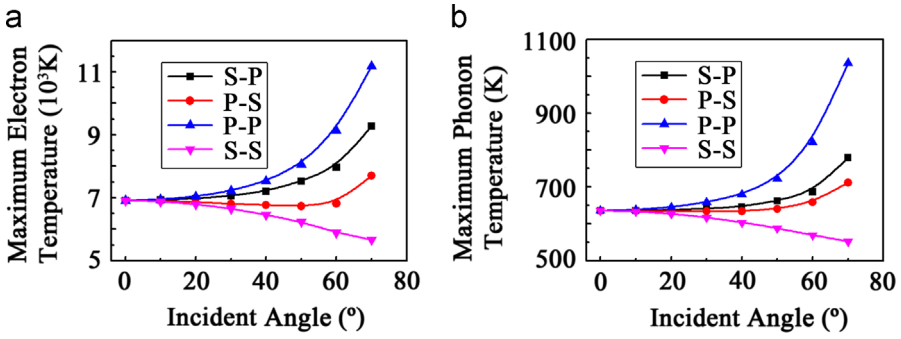

Fig. 4. The maximum electron and the maximum phonon temperatures on the Au film surface as a function of the incident angle for polarization-shaped double-pulses for with s–p, p–s, p–p, and s–s polarization combinations. The laser fluence F=0. 15 J/cm^2, pulse duration t_p=100 fs, laser wavelength λ=800 nm, pulse separation Δ=2.5 ps. (a) Maximum electron temperature. (b) Maximum phonon temperature.

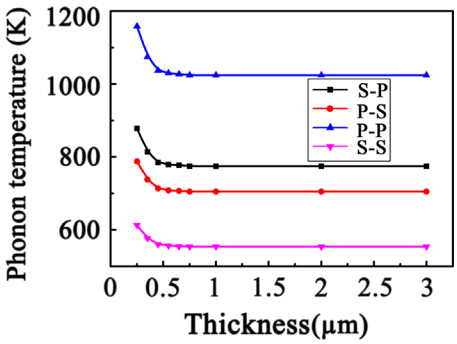

Fig. 6. The maximum phonon temperature on the Au film surface as a function of the thickness for polarization-shaped double-pulses with s–p, p–s, p–p, and s–s polarization combinations. The laser fluence $F=0.\ 2\ J/cm^2$, pulse duration $t_p=100$ fs, laser wavelength $\lambda=800$ nm, pulse separation $\Delta=2.5$ ps, incident angle $\theta=70^\circ$.

tuned by optimizing the double-pulse polarization combination with respect to the incident angle. This opens a new route for enhancing the optimal laser energy deposition into the Au target by tailoring the polarization state of a temporally shaped femtosecond laser.

The maximum phonon temperature on the Au film as a function of the thickness for polarization-shaped double-pulses with s–p, p–s, p–p, and s–s polarization combinations are shown in Fig. 6. The maximum phonon temperature decreases gradually with the increase of the thickness of Au film when the thickness of Au film less than 0.75 μm. However, the maximum phonon temperature is almost constant when the thickness exceeds 0.75 μm. For the p–p polarization combination, the maximum phonon temperature is higher than that for other polarization combinations. When the thickness is less than 0.75 μm, the phonon temperature is higher because there is less material initially at room temperature to absorb energy from the heated zone. Thus, less thickness leads to a higher temperature rise. When the thickness is greater than 0.75 μm, the film thickness has little influence on the maximum phonon temperature. Experiments show that the damage threshold increases with increasing film thickness, which indirectly demonstrates that the maximum phonon temperature on the Au film surface decreases with increasing film thickness when the laser energy is fixed [23]. This verifies the validity of the simulated results.

4. Conclusion

This study theoretically investigated the ultrafast thermalisation dynamics in an Au film irradiated by polarization-shaped femtosecond laser double-pulses. It is revealed that the phonon temperature of the Au film excited by a double-pulse with the p–p double-polarization combination is superior to that from other double-polarization combinations (s–s, s–p, and p–s polarization combinations). The mechanism that leads to this enhancement is related to the higher energy absorption efficiency of the double-pulse with the p–p polarization combination. Further, the two-temperature relaxation time can be flexibly tuned by using the optimal polarization combination for a given incident angle. In addition, the maximum phonon temperature decreases gradually with the increase of the thickness of the Au film when the thickness of the Au film less than 0.75 μm and the maximum phonon temperature for the p–p polarization combination is higher than that for other polarization combination. The study provides the basic strategy for improving the thermalization efficiency of femtosecond high-precision laser fabrication by tailoring the polarization state of a temporally shaped femtosecond laser pulse.

Acknowledgments

This work is supported by the National Science Foundation of China under the Grant Nos. 61275008, 11404254, 51335008 and 61176113, the Special-funded programmer on national key scientific instruments and equipment development of China under the Grant No. 2012YQ12004706.

References

[1] Hu YL, Chen YH, Ma JQ, Li JW, Huang WH, Chu JR. High-efficiency fabrication of aspheric microlens arrays by holographic femtosecond laser-induced photopolymerization. Appl Phys Lett 2013;103:141112.
[2] Camino A, Hao ZQ, Liu X, Lin JQ. High spectral power femtosecond supercontinuum source by use of microlens array. Opt Lett 2014;39:747–50.
[3] He SG, Chen F, Yang Q, Liu K, Shan C, Bian H, et al. Facile fabrication of true three-dimensional microcoils inside fused silica by a femtosecond laser. J Micromech Microeng 2012;22:105017.
[4] Liao Y, Ju YF, Zhang L, He F, Zhang Q, Shen YL, et al. Three-dimensional microfluidic channel with arbitrary length and configuration abricated inside glass by femtosecond laser direct writing. Opt Lett 2010;35:3225–7.
[5] Jiang L, Zhao LJ, Wang S, Yang JP, Xiao H. Femtosecond laser fabricated all-opticalfiber sensors with ultrahigh refractive index sensitivity: modeling and experiment. Opt Express. 2011;19:17591–8.
[6] Korte F, Nolte S, Chichkow BN, Bauer T, Kamlage G, Wagner T, et al. Far-field and near-field material processing with femtosecond laser pulses. Appl Phys A. 1999;69:s7–11.
[7] Momma C, Nolte S, Chickov BN, Alvensleben FV, Tunnermann A. Precise laser ablation with ultrashort pulses. Appl Surf Sci 1997;109:15–9.
[8] Chichkov BN, Momma C, Nolte S, von Alvensleben F, Femtosecond Tunnermann A. picosecond and nanosecond laser ablation of solids. Appl Phys A 1996;63:109–15.
[9] Luft A, Fanz U, Emsermann A, Kaspar J. A study of thermal and mechanical effects on materials induced by pulsed laser drilling. Appl Phys A 1996;63:93–101.
[10] Harzic RL, Breitling D, Weikert M, Sommer S, Fohl C, Dausinger F, et al. Ablation comparison with low and high energy densities for Cu and Al withultra-short laser pulses. Appl Phys A 2005;80:1589–93.
[11] Harzic RL, Audouard NE, Jonin C, Laporte P, Valette S, Fraczkiewicz A, et al. Comparison of heat-affected zones due to nanosecond and femtosecond laser pulses using transmission electronic microscopy. Appl Phys Lett 2002;80:3886–8.
[12] Jiao LS, Ng EYK, Wee LM, Zheng HY. Role of volatile liquids in debris and hole taper angle reduction during femtosecond laser drilling of silicon. Appl Phys 2011;104:1081–4.
[13] Stoian R, Boyle M, Thoss A, Rosenfeld A, Korn G, Hertel IV, et al. Laser ablation of dielectrics with temporally shaped femtosecond pulses. Appl Phys Lett 2002;80:353–5.
[14] Donnelly T, Lunney JG, Amoruso S, Bruzzese R, Wang X, Ni X. Double pulse ultrafast laser ablation of nickel in vacuum. J Appl Phys 2009;106:013304.
[15] Semerok A, Dutouquet C. Ultrashort double pulse laser ablation of metals. Thin Solid Films 2004;453–4:501–5.
[16] Leng N, Jiang L, Li X, Xu CC, Liu PJ, Lu YF. Femtosecond laser processing of fused silica and aluminum based on electron dynamics control by shaping pulse trains. Appl Phys A 2012;109:679–84.
[17] Jiang L, Tsai HL. Modeling of ultrashort laser pulse-train processing of metal thin films. Int J Heat Mass Transfer 2007;50:3461–70.
[18] Sim HS, Park S, Kim TH, Choi YK, Lee JS, lee SH. Femtosecond laser pulse train effect on optical characteristics and nonequilibrium heat transfer in thin metal films. Mater Trans 2010;51:1156–62.
[19] Du GQ, Chen F, Yang Q, Si JH, Hou X. Ultrafast thermalization characteristics in Au film irradiated by temporally shaped femtosecond laser pulses. Opt Commun 2011;284:640–5.
[20] Anisimov SI, Kapeliovich BL, Perel'man TL. Electron emission from metal surfaces exposed to ultrashort laser pulses. JETP 1974;39:375–7.
[21] Nolte S, Momma C, Kamlage G, Ostendorf A, Fallnich C, von Alvensleben F, et al. Polarization effects in ultrashort-pulse laser drilling. Appl Phys A 1999;68:563–7.
[22] Chen AM, Xu HF, Jiang YF, Sui LZ, Ding DJ, Liu H, et al. Modeling of femtosecond laser damage threshold on the two-layer metal films. J. Appl Surf Sci 2010;257:1678–83.
[23] Stuart BC, Feit MD, Herman S, Rubenchik AM, Shor BW, Perry MD. Optical ablation by high-power short-pulse lasers. J Opt Soc Am B 1996;13:459–68.